ROYAL SOCIETY
OF **CHEMISTRY**

PAPER
Hwajin Kim *et al.*
Chemical characterization and formation of secondary
organosiloxane aerosol (SOSiA) from OH oxidation
of decamethylcyclopentasiloxane

PAPER

Check for updates

Chemical characterization and formation of secondary organosiloxane aerosol (SOSiA) from OH oxidation of decamethylcyclopentasiloxane†

Yanfang Chen, [ID] [ab] Yoojin Park,[c] Hyun Gu Kang, [ID] [d] Jiwoo Jeong[a] and Hwajin Kim [ID] *[ab]

Cyclic volatile methyl siloxanes (cVMS) are anthropogenic chemicals emitted by consumer and industrial products. Evidence from laboratory and ambient studies indicates that cVMS contribute to the formation of secondary organosiloxane aerosol (SOSiA). However, the oxidation products and formation pathway under various atmospheric conditions have yet to be clarified. To address these knowledge gaps, we generated SOSiA from the OH oxidation of decamethylcyclopentasiloxane (D_5-siloxane, ~200 ppb) in a potential aerosol mass oxidation flow reactor (PAM-OFR, 185 mode) with the photochemical aging from 0.51–7.04 days. The chemical composition of SOSiA was characterized with an online high-resolution time-of-flight aerosol mass spectrometer (HR-ToF-AMS) and offline electrospray ionization mass spectrometry (ESI-MS). A series of high-molecular-weight SOSiA ions were observed in the AMS mass spectra. Using the ESI-MS analysis, molecular identification of D_5-siloxane oxidation products was provided, allowing us to propose the possible formation pathways of the major products. Our results show the combination of multiple mass spectrometry techniques may further offer new insights into characterizing SOSiA-related species and can be used to identify SOSiA tracers from ambient measurements both indoors and outdoors.

Environmental significance

As an important anthropogenic volatile organic compounds (VOCs) source, cyclic volatile methylsiloxane (cVMS) species are regarded as significant contributors influencing indoor and urban air quality. However, the environmental fate of siloxanes is poorly understood. Our results demonstrate that online high-resolution time-of-flight aerosol mass spectrometer (HR-ToF-AMS) is able to detect secondary organosiloxane aerosol (SOSiA), thus can be used to identify SOSiA tracer from ambient measurements both indoors and outdoors in the future. The possible formation pathways of D_5 SOA were proposed to better understand the atmospheric chemistry of siloxane compounds.

1. Introduction

Cyclic volatile methyl siloxanes (cVMS) are anthropogenic chemicals emitted from many personal care and industrial products[1] and are thus considered important volatile organic compound (VOC) sources in urban atmospheres[2] and indoor environments.[3] Due to the high saturation vapor pressures and low water solubility, most of the cVMS species preferentially partition to the atmosphere. Recent studies[4,5] have found that the enhancements of cVMS in U.S. cities generally correlated with population density. In addition, cVMS have been detected in rural and remote regions due to long-range transport.[6] They have been also detected in water, soil, sediments and biota due to their widespread use in consumer products.[7]

The cVMS could undergo further gas-phase oxidation to form new products in the atmosphere.[8,9] The dominant cVMS oxidation involves reactions with hydroxyl radicals (OH) and chlorine atoms (Cl), which oxidize cVMS on the timescale of

[a]*Department of Environmental Health Sciences, Graduate School of Public Health, Seoul National University, 08826 Seoul, South Korea. E-mail: khj0116@snu.ac.kr*

[b]*Institute of Health and Environment, Graduate School of Public Health, Seoul National University, 08826 Seoul, South Korea*

[c]*Department of Environmental Science and Engineering, College of Engineering, Ewha Womans University, 03760 Seoul, South Korea*

[d]*Multiphase Chemistry Department, Max Planck Institute for Chemistry, 55128 Mainz, Germany*

† Electronic supplementary information (ESI) available: Details of the experimental conditions (Table S1†). Formulas of D_5-SOSiA AMS fragments and identified molecular composition (Table S2 and S3†). Comparison between modeled and measured OH_{exp} and O_3 concentrations (Fig. S1†). Representative time series from PAM-OFR experiments (Fig. S2†). AMS high-resolution mass spectra and raw UMR mass spectra (Fig. S3 and S4†). ESI-MS (−) mass spectrum of blank filter and SOSiA compounds (Fig. S5 and S6†). Possible structures of identified SOSiA compounds from ESI-MS (Fig. S7–S10†). See DOI: https://doi.org/10.1039/d2ea00161f

a couple of days, and the reactions with nitrate radicals (NO_3) and ozone (O_3) are negligible.[10] Additionally, cVMS oxidation products, such as silanols, are also likely to have long atmospheric lifetimes and thus are also likely to undergo further oxidation in the atmosphere.[11] Currently, cVMS are exempt from VOC regulations in the United States,[12] despite their potential health and climate implications. Fu et al.[13] found high formaldehyde (HCHO) yield through cVMS oxidation, which could lead to significant ozone formation. Due to the properties of persistent, bioaccumulative, toxic and long-range atmospheric transport, cVMS are currently being considered as emerging persistent organic pollutants (POPs) for regulation.[14]

Recent results have also detected low-volatility siloxanes in the particle phase from indoor cooking events[15] or ship emissions.[16] Evidence from laboratory studies indicated that oxidized cVMS products could also contribute to the formation of secondary organosiloxane aerosol (SOSiA),[17,18] especially decamethylcyclopentasiloxane (D_5-siloxane, $C_{10}H_{30}O_5Si_5$), the most abundant siloxane in urban areas.[19] However, the reported SOA yields varied significantly between different literature reports. Wu and Johnston[17] found that the presence of seeds can enhance the SOA yields from 7.9 to 23.1%, while the SOA yields reported by Han et al.[20] did not show significant enhancement with seed aerosol. A recent study[21] highlighted that the D_5-siloxane SOA yields are strongly dependent on either the OH concentration or exposure. Under low OH concentrations and exposures, the SOA yield was found to be negligible, while the yields can reach 110% at higher OH mixing ratios. However, it should be noted that the OH concentration and exposure are not necessarily interchangeable,[22] and the two parameters may cause different influences on SOA formation. In addition, as oxidation products were not reported in this previous study, the oxidation products and formation mechanism under various atmospheric conditions have yet to be clarified.

A few previous studies have investigated the chemical composition and formation mechanism of D_5-SOSiA. Janechek et al.[23] characterized the elemental composition of SOSiA and found the presence of Si in the filter samples via energy-dispersive X-ray spectroscopy (STEM-EDS). Chandramouli and Kamens[24] also confirmed that the main product of SOSiA is silanol (D_4T-OH, "D" refers to the units of $(CH_3)_2SiO$ and "T" refers to CH_3SiO) by Gas Chromatograph (GC). Wu and Johnston[17,25] identified three main types of SOSiA species, including ring-opening products, monomers and dimers with high-performance mass spectrometry in both negative ([M − H]$^-$) and positive ([M + H]$^+$ and [M + Na]$^+$) ion mode, and the oxidation mechanism was also proposed based on the main products. To date, the number of studies investigating the chemical composition of SOSiA is extreme limited compared to the number of studies on SOSiA yield, resulting in larger uncertainties in D_5 oxidation mechanisms. Such missing information hinders a comprehensive understanding of the environmental fate and impact of cVMS.

Several studies have also detected SOSiA species from filter samples collected from outdoor ambient air. Milani et al.[26] have detected and quantified the D_4T-OH in ambient particulate

matter (PM) based on gas chromatography coupled with mass spectrometry (GC-MS) analysis, but the total SOSiA mass concentration remains unquantified. Xu et al.[27] established a quantitative approach to investigate SOSiA in ambient $PM_{2.5}$ samples. However, so far, little is known the temporal dynamics information of SOSiA, therefore, analytical instrumentation that can provide real-time characterization of SOSiA is required to elucidate the formation and evolution process.

To our knowledge, the only real-time instrument applied for the characterization of SOSiA to date is the Aerodyne High-Resolution Time-of-Flight Aerosol Mass Spectrometer (HR-ToF-AMS).[28] Han et al.[20] conducted a series of oxidation flow reactor (OFR) experiments to investigate the SOSiA generated from OH oxidation of cVMS. Although SOSiA ions ($C_wH_xO_ySi_z^+$) were observed in the AMS mass spectra, only the dominant fragment ions in the low m/z (<420) range were detected. Since the dimer oxidation products of D_5-siloxane have also been reported in a previous study,[25] the high-molecular-weight SOSiAs (>m/z 420) have likely been largely ignored due to the limited detection range of AMS. The dominant peaks at m/z 327 and 329 were assigned as $C_{12}H_{11}O_2Si_5^+$ and $C_9H_9O_8Si_3^+$ in the AMS mass spectra. However, the parent siloxane has the structure of $(SiO(CH_3)_2)_5$ with the C/Si ratio of 2, whereas the assignments in this previous study appear to deviate from the structures of oxidation products (e.g., D_4T-OH and D_4T-CH_2OH). This conflict is also likely due to the ambiguous identifications of oxidation products and unknown mechanisms. This requires a further investigation of the parent molecular composition of SOSiA fragments observed in AMS.

Herein, we carried out a series of OFR experiments to investigate the SOSiA generated from the OH oxidation of D_5-siloxane under various OH exposure (OH_{exp}) regimes. Two state-of-the-art mass spectrometry techniques, including online HR-ToF-AMS and offline electrospray ionization mass spectrometry (ESI-MS), are used to gain insight into the chemical composition and formation pathway of SOSiA.

2. Experimental

2.1. Oxidation flow reactor (OFR) experiments

The oxidation experiments presented in this work were carried out in a potential aerosol mass oxidation flow reactor (PAM-OFR, Aerodyne Research, USA).[29,30] The volume of the OFR is 13.3 L, and the total flow rate in the OFR was set to 4.43 L min^{-1} using mass flow controllers (Alicat Scientific, USA), leading to a residence time of 180 s in the OFR. The "OFR185 mode" was used to generated OH radical via photolysis of H_2O and O_2 at λ = 185 nm plus photolysis of O_3 at λ = 254 nm.[31] Nitrogen gas (N_2, 30 psig) was flushed into the sleeves to cool the lamps and minimize artifact oxidant formation around the lamps. Prior to each experiment, the OFR was flushed with humidified zero air with 185 nm lamp turned on overnight to clean the system. D_5-Siloxane (97%, Sigma-Aldrich, USA) was continuously injected into a glass bulb using a syringe pump (Fusion 4000, Chemyx, USA), followed by flowing zero air (Model 8301P zero air generator; Model HTO-1000HC catalytic converter, Acoem Ecotech, Victoria, Australia) to achieve a mixing ratio of ∼200 ppb

© 2023 The Author(s). Published by the Royal Society of Chemistry

Environ. Sci.: Atmos., 2023, **3**, 662–671 | **663**

in the OFR. All experiments were carried out in the absence of seed aerosol at room temperature, and the relative humidity (RH) inside the OFR was varied by adjusting the flow ratio of dry air and wet air through a humidifier (FC-100-80-6MKK, Perma Pure, USA). The OH_{exp} is controlled by regulating the lamp voltages and the RH in the PAM. The detailed experimental condition for each experiment are illustrated in ESI Table S1.† The OH_{exp} for each experiment conditions was obtained by the decay of carbon monoxide (CO) gas inside the OFR using CO analyzer (Serinus 30, Ecotech, Australia) during separate offline calibrations.[32] Details about the comparison between modeled and measured results of OH_{exp} calibration can be found in Fig. S1.†

As Peng et al.[33] pointed out, OFR185 requires low UV intensity, low external OH reactivity (OHR_{ext}) (<30 s^{-1}) and high H_2O mixing ratio (>0.8%) to keep both VOC and RO_2 chemistries to be atmospherically relevant. In order to ensure the OFR 185 was operated under "safer conditions", the two low-pressure germicidal Hg lamps (GPH436T5VH, Light Sources, USA) were wrapped by segmented heat shrink tubing, and 90% of the lamp surface was covered to achieve low UV intensity. We followed the instructions of Rowe et al.[34] to calculate the photon fluxes at 185 and 254 nm (I_{185} and I_{254}), the maximum I_{254} (I_{254max}) of 3.0 × 10^{15} photons cm^{-2} s^{-1} and I_{185max}/I_{254max} ratio of 0.0664 were assumed in this study. The estimated I_{185} and I_{254} are to be in the ranges of 3.70 × 10^{12}–1.64 × 10^{13} and 2.05 × 10^{13}–2.64 × 10^{14} photons cm^{-2} s^{-1}, respectively.

The UV photolysis lifetime (t_photol) of D_5 was calculated using the following equation (https://sites.google.com/site/pamwiki/pam-time-constants):

$$t\_photol = \frac{1}{sigma \times UV\_flux}$$

where UV_flux represents the photon flux (photons cm^{-2} s^{-1}) in PAM, sigma represents the absorption cross section (cm^2) of the oxidant precursor. We assumed I_{185max} = 1.64 × 10^{13} photons cm^{-2} s^{-1}. Since the absorption cross section at 185 nm for D_5 was not available from literature, we assumed the value to be 5.36 × 10^{-18} cm^2 based on octamethylcyclotetrasiloxane (D_4).[35] Corresponding t_photol value was 11 370 s, which is much higher than the residence time (180 s) of the PAM-OFR. Bernard et al. also pointed out,[35] the siloxane photolysis at 248 nm was negligible. Thus, we believe the contribution of photolysis at 185 and 254 nm to D_5 should be negligible.

In addition, since UV and OH production is relatively low, H_2O vapor was injected into the PAM across all experiments, the corresponding water vapor mixing ratio (H_2O) were ~0.8% and ~2.2% for 30% RH and 80% RH experiments respectively. The low OHR_{ext} (~9.8 s^{-1}, initial D_5 concentrations ([D_5]$_{init}$ of 200 ppb) is also used to avoid OH suppression.

Under these preferred conditions, the OH_{exp} in OFR185 ranged from 6.57 × 10^{10} to 9.12 × 10^{11} molecules cm^{-3} s, equivalent to the photochemical age of 0.51 to 7.04 days. Although the OH concentrations in OFR are much higher than those in the ambient atmosphere, considering the half-life of D_5 (3.5–7 days), we believe that the range of OH_{exp} covered by our study is atmospherically relevant. Since we did not conduct

experiments under high NO_x conditions, the experimental conditions used in our study may only represent the atmospheric scenarios with few NO_x sources. Further studies are needed to acquire a quantitative understanding of the role of NO_x in SOSiA formation.

2.2. Online instrumentation

To minimize the gas and particle loss and avoid siloxane contamination,[36] conductive perfluoroalkoxy alkane (PFA) tubing (1/4″ OD, Fluorotherm Polymers, USA) and PFA (1/4″ OD, Sungjin Rubber, South Korea) tubing were used through the OFR inlet and sampling line. The particle number concentrations and size distributions were measured continuously with a scanning mobility particle sizer (SMPS, Classifier Model 3082, Ultrafine Condensation Particle Counter Model 3756, TSI, USA). The SMPS was operated with an aerosol flow rate of 0.3 L min^{-1} and a sheath flow of 1.5 L min^{-1}. The size distribution (mobility diameter = 22.9–1000 nm) scan time was set to 120 s, with 5 s retrace, 10 s purge and 45 s wait time between scans (180 s total). The particle composition was measured with a HR-ToF-AMS (Aerodyne Research, USA). The AMS was operated with a pulse time of 65 μs (typical pulser periods: ~40 μs), allowing for m/z range up to 1080. Since we expanded the m/z range, it would reduce the number of MS data points and the overall sensitivity, only V mode was used instead of W mode. Note that the PToF mode was also not available in this study. AMS was carefully tuned and optimized following the standard procedures to achieve the sensitivity and resolution. During the experiment, the ionization efficiency (IE) calibration and filter blank measurement were performed following standard protocols. AMS data was analyzed with Squirrel (v. 1.64 A) and Pika (v. 1.24 A) in Igor Pro (v. 8.0.4.2). The AMS HR ion list was modified to include Si-containing fragments and their corresponding isotopic ions using the HR ion mass calculator in Pika.

Gas-phase concentrations of D_5-siloxane were measured using a proton transfer reaction mass spectrometer (PTR-ToF 1000, Ionicon Analytik, Austria). The PTR-MS used the H_3O^+ ion source as the reagent ions. The voltage of U_{drift} was set to 525 V, resulting an E/N of 120 T. The temperatures of drift tube and inlet line were set to 80 °C. Mixed standards gas (Apel-Riemer Environmental, USA) was used for PTR-MS calibration. O_3 concentrations were measured downstream of the OFR using an O_3 analyzer (Model UV-100, 2B Technologies, USA).

2.3. Offline ESI-MS analysis

2.3.1. Filter collection. The SOSiA particles were collected onto Teflon polytetrafluoroethylene filters (PTFE, PT48P-KR, Minneapolis, MN, USA) using a stainless steel 47 mm inline filter holder (Pall Life Sciences, USA) for off-line analysis. The sampling was performed after the start of particle formation for 15 minutes at flow rate of 3 L min^{-1} for 4–10 hours depending on the particle concentration in the OFR. The time series from two representative PAM-OFR experiments can be found in Fig. S2.† The O_3 denuder filled with hopcalite pellets (3 mm, Purelyst MD-101, Pure Sphere, South Korea) was installed before the SMPS and filter sampling line to remove the high O_3

664 | Environ. Sci.: Atmos., 2023, **3**, 662–671

© 2023 The Author(s). Published by the Royal Society of Chemistry

from output of the OFR. The measured removal efficiency by the denuder was ~90% for test experiment, with initial O_3 concentration at 2.1 ppm. Prior to experiments, the O_3 denuder was purged using clean air, we did not observe particles from the O_3 denuder during background check experiments. The filters were weighed before and after particle collection using a semi-micro balance (QUINTIX125D-1SKR, Satorius, Germany).

2.3.2. Filter extraction procedure. Each filter was placed in a clean bottle and extracted with 10 mL acetonitrile (HPLC grade, ≥99.9%, Sigma-Aldrich, USA) three times followed by 10 minutes of sonication. The extracts were filtered through a 0.45 μm PTFE syringe filter and transferred to another clean vial, then ~10 mL of acetonitrile was added. The resulting solutions were concentrated under a gentle stream of N_2 at room temperature to a volume of ~1 mL, then ~1 mL of acetonitrile was added to the extracts.

2.3.3. ESI-MS operation. The extracted samples were further analyzed for molecular composition using a High Definition Mass Spectrometry System (Synapt-G2, Waters, US) equipped with an electrospray ionization source (ESI). The ESI-MS analysis was carried out in both positive (ESI-MS (+)) and negative ion (ESI-MS (−)) modes with a direct-infusion method. The mass spectrometer was operated in resolution mode with a full width at half maximum mass resolving power of 20 000. The optimized MS parameters were as follows: the capillary voltage of 2 kV, sampling cone voltage of 40 V, source temperature of 120 °C. The desolvation gas flow rate was 800 L h^{-1} at 350 °C and the cone gas flow was 100 L h^{-1}. The collision energies were set to 4 eV in low energy mode. All the data acquisition was performed in the continuum mode at the mass range of m/z 50–1200 with MassLynx software (v4.1, Waters, US). Leucine enkephalin ($C_{28}H_{37}N_5O_7$, m/z 556.2771 for ESI-MS (+) and m/z 554.2615 for ESI-MS (−)) was used as a lock mass calibrator in all analyses to obtain accurate masses. The obtained mass accuracy for leucine enkephalin was performed within ±0.5 ppm mass error. Mass spectra for blank filter extracts were measured using the same method. No authentic standard was used to quantify the analytes since there is no commercially available standard.

2.3.4. ESI-MS data processing. The ESI-MS datasets were further processed using the UniFi software (v1.8, Waters, US). The initial peak assignments were limited to: C, H, O and Si containing formulae as these were expected products from siloxane oxidation chemistry. The mass tolerance was initially set at 10 ppm. The I-FIT isotope predictive filtering was also used to reduce the number of proposed elemental compositions. Sodiated ions [M + Na]$^+$ and protonated ions [M + H]$^+$ were assigned to identify products detected in the ESI-MS (+) mode. Deprotonated ions [M − H]$^-$ were assigned in the ESI-MS (−) mode. The final assigned reasonable formulae were constrained by a mass error of mostly <5 ppm.

2.4. Pure D_5 particle generation experiment

For comparison, laboratory experiments were carried out to detect the pure D_5-siloxane particles with AMS. The particles were generated by atomizing diluted D_5-siloxane solution using a constant output atomizer (model 3076, TSI, US) with zero air. Isopropanol (≥99.5%, Sigma-Aldrich, USA) was used as solvent for D_5-siloxane. The AMS was operated with a silica gel diffusion dryer in front of the sampling line to keep RH lower than 30%.

3. Results and discussion

3.1. Bulk characterization of the secondary organosiloxane aerosol using AMS

Fig. 1a shows the unit mass resolution (UMR) mass spectra of D_5-SOSiA measured by AMS. The dominant ions were distributed in the low m/z range (m/z < 550, 96.05%), and the SOSiA spectra were dominated by signals at m/z 73 ($C_3H_9Si^+$), 327 ($C_5H_{15}O_7Si_5^+$) and 329 ($C_4H_{13}O_8Si_5^+$). A series of distinct peaks at m/z 147 ($C_5H_{15}OSi_2^+$), 207 ($C_5H_{15}O_3Si_3^+$), 221 ($C_7H_{21}O_2Si_3^+$), 267 ($C_5H_{15}O_5Si_4^+$), 281 ($C_7H_{21}O_4Si_4^+$), 295 ($C_9H_{27}O_3Si_4^+$), 341 ($C_7H_{21}O_6Si_5^+$), and 355 ($C_9H_{27}O_5Si_5^+$) were also observed. These ions have been reported as common fragments of siloxane compounds.[37] For comparison, the mass spectrum of the pure D_5-siloxane standard with isopropanol solvent was also measured and is shown in Fig. 1b. Although the parent molecules of SOSiA and pure D_5-siloxane (MW: 370.77 g mol^{-1}) are different, in addition to some small fragments from

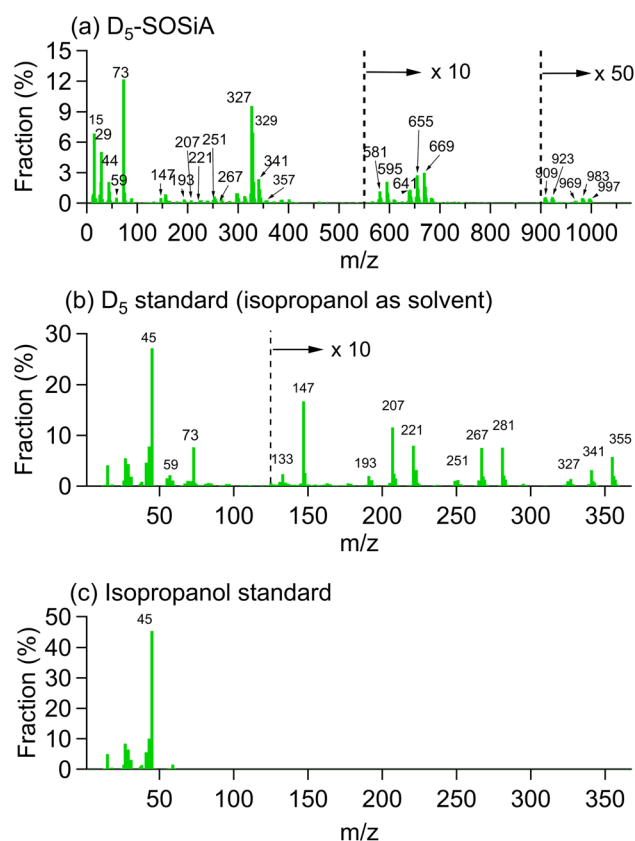**Fig. 1** Normalized AMS mass spectra of (a) D_5-SOSiA generated from the OH oxidation experiment at the stable stage, (b) pure D_5-siloxane standard with isopropanol solvent and (c) pure isopropanol generated from atomizer. All the spectra are shown as stacked at unit mass resolution.

© 2023 The Author(s). Published by the Royal Society of Chemistry

Environ. Sci.: Atmos., 2023, **3**, 662–671 | **665**

isopropanol (Fig. 1c), similar distinctive ion patterns were observed, further confirming that the dominant fragment ions are representative of Si-containing OA.

Although the ability of AMS to characterize molecular composition is limited, several Si-containing fragments (C_wH_x-$O_ySi_z^+$) in the low m/z range (for example, m/z 73 and 147 shown in Fig. S3†) were confirmed in AMS mass spectra using HR peak fitting. The isotope ions of $C_3H_9Si^+$ at m/z 74 ($C_3H_9{}^{29}Si$ and $^{13}CC_2H_9Si$) also fit well. However, it must be noted that due to the limited mass resolution ($m/\Delta m \sim 2000$ for V mode) of the AMS, the HR fitting parameters are incapable of resolving C_w-$H_xO_ySi_z^+$ ions in the high m/z range (>m/z 200), as it is difficult to robustly resolve the surrounding ions due to the large number of possible formulae. Furthermore, the mass calibration may be largely unconstrained in the high m/z range. Given the uncertainties and limitations, we only reported the UMR mass spectra in this study. Fig. S4a† shows examples of raw mass spectra of the D_5 standard detected from AMS along with the expected isotopic ratios calculated from the isotope distribution calculator (https://www.sisweb.com/mstools/isotope.htm). The ion distributions typically include five m/z values, with one parent peak and four isotope ions. The intensity ratios between the parent peak and isotope ions match exactly the expected isotopic ratios, thus unequivocally confirming the detection of Si-containing particles. Analogous to the D_5 standard, a similar isotope distribution was observed from D_5-SOSiA (Fig. S4b†) with disparities in signal intensity, suggesting that more Si-containing fragments (even if they overlap with isotope ions) were generated from secondary oxidation products. The possible formulae of $C_wH_xO_ySi_z^+$ ions are listed in Table S2.†

Several large ions (e.g., m/z = 550–750, 3.78%; m/z > 900, 0.17%) were also observed in the mass spectra. A clear separation by 74 mass units between adjacent peaks was observed, e.g., m/z 581 and 655, m/z 595 and 669, m/z 909 and 983, m/z 923 and 997. The 74 mass units may correspond to the dimethyl siloxane unit ($SiO(CH_3)_2$, m/z 74.0188). The separation with the 254 ($C_6H_{18}O_5Si_3$, m/z 254.0462) mass units were also observed between SOSiA fragments, (e.g., m/z 73, 327 and 581, m/z 655 and 909, m/z 669 and 923), indicating that these fragments are Si-containing ions. Although it is well known that AMS is limited by its flash vaporization (600 °C) and high energy electron ionization (70 eV), which break the high-molecular-weight compounds into extensive fragments. Due to the low volatility, it is likely that high-molecular-weight SOSiAs may not be completely vaporized by the AMS. A few previous field[38] and laboratory[39] studies have also reported that AMS can be used for detecting high mass ions (up to $\sim m/z$ 2000 for fullerene ions). Previous studies have clearly shown that D_5-siloxane oligomers have been observed in the particle phase,[17,25] and the large-molecular-weight fragments observed in AMS mass spectra may also provide evidence of D_5-SOSiA oligomers.

To our knowledge, this work is the first demonstration of the use of AMS for the measurement of high-molecular-weight SOSiA ions. Taken together, we believe that AMS can detect SOSiA-related species and can further be used to identify SOSiA tracers from ambient measurements. However, the SOSiA fragment ions detected with AMS could not provide the

molecular composition or the formation mechanisms of SOSiA. Thus, further experiments were conducted to confirm the molecular composition of SOSiA using ESI-MS, which is a softer ionization technique than AMS. The results will be described in more detail in the following section.

3.2. Molecular characterization of the secondary organosiloxane aerosol

3.2.1. ESI-MS mass spectrum. Due to the higher sensitivity (ionization efficiency) and lower detection limits with the ESI-MS negative ion mode,[40] this work mainly reports the ESI-MS data acquired in the negative mode (ESI-MS (−)). The ESI-MS (−) mass spectra of the blank filter and D_5-SOSiA are shown in Fig. S5 and S6.† Except for the lowest OH_{exp} condition, D_5-SOSiA appears to have similar mass spectra with a clear grouping of peaks in different m/z ranges, i.e., m/z < 400 and m/z 400–800; these distributions are also consistent with the fragments observed in the AMS mass spectra (Fig. 1a). For example, the abundant fragments at m/z 327 ($C_5H_{15}O_7Si_5^+$) and m/z 329 ($C_4H_{13}O_8Si_5^+$) observed in AMS may correspond to the dominant molecular ions at m/z 358 ($C_7H_{22}O_7Si_5$) and m/z 360 ($C_6H_{20}O_8Si_5$) with the loss of two CH_3 groups and a hydrogen shift. It is important to note that the fragments of m/z 327 and 329 from SOSiA measured by AMS have been previously[20] identified as $C_{12}H_{11}O_2Si_5^+$ and $C_9H_9O_8Si_3^+$, which may have differences in the inferred fragments from our studies. Due to the extensive fragmentation and the electron impact ionization processes, it is difficult to determine the relationship of all the fragments and parent ions. Although we are not able to provide the chemical information of the AMS fragments above m/z 500, these fragments may correspond to the ions between m/z 550 and m/z 800 in ESI-MS (−). The AMS fragments above m/z 800 were not observed in ESI-MS (−). It is likely that the ESI-MS (−) results shown here are biased toward the species with higher ionization efficiencies in ESI, which may be more limited in the compounds it can detect than AMS.

Table S3† lists the assigned molecules observed in the ESI-MS (−) mass spectra. Most of these compounds were identified as ring-opening products, which were defined as those containing neither 5 nor 10 Si atoms. The compounds containing 5 or 10 Si atoms but with additional unsaturated bonds (e.g., Si=O) were also defined as ring-opening products. For example, we identified some small silanols (DT-OH, D_2T-OH and D_3T-OH) and their further oxidation products (siloxandiols, DT_2-(OH)$_2$ and D_2T_2-(OH)$_2$). Possible structures of these products are shown in Fig. S7.† Silanol products have been regarded as first-generation products.[25] Previous studies have also reported that silanol can be formed from the hydrolysis of formate ester,[8,41] and silanols continue to undergo hydrolysis to produce smaller silanols.[42] Since the oxidation experiments were performed at 30% and 80% RH, it is likely that hydrolysis reactions may occur at the surface of the SOSiA or the OFR wall. The dominant ring-opening products were assigned as $C_7H_{22}O_7Si_5$ and $C_6H_{20}O_8Si_5$. Although we were not able to explore the possible structures of these products and their isomers with further analysis (e.g., ESI-MS/MS analysis),

666 | Environ. Sci.: Atmos., 2023, 3, 662–671

© 2023 The Author(s). Published by the Royal Society of Chemistry

the structure of the ring-opening products (with Si=O) have been previously confirmed from tandem mass spectrometry analysis.[17] Thus, we suspect that they may constitute OH groups (with the replacement of CH_3 groups) and an additional unsaturated site (Si=O) (Fig. S8†).

The major difference between previous studies and our results is the substantial presence of ring-opening products. Although Wu and Johnston[17] found relatively high signal intensities of ring-opening products at low SOSiA mass loading (1.2 μg m^{-3}), these compounds were considered to have minor contributions at higher aerosol mass for the unseeded experiments. In our case, the ring-opening products comprise a significant portion of the SOSiA contribution regardless of the mass loading (from 20 to ~1000 μg m^{-3}). A possible explanation for the large changes in the chemical composition between our results and those of a previous study may be related to the water content between experiments. In previous study,[17] the experiments were performed with low RH (8–10%); in our experiments, water is added into the OFR (~30% and 80%) to make OH radicals. It has been shown that relative humidity does affect the gas-phase oxidation products of D_4.[43] Additionally, previous work also proposed the humidity-dependent mechanism for the gas-phase OH/Cl oxidation of D_3.[11] Avery et al.[44] found the RO_2 fates varied across dry and humid conditions for Cl oxidation of D_5, while the effect of humidity on SOA yields and chemical composition were also observed in their study. Thus, we believe that the high humidity could affect the D_5 oxidation mechanism.

Although we could not unambiguously identify the ring-opening products from our PTR-MS measurement, Wu and Johnston identified ions indicative of ring-opening in their mass spectrometry analysis of SOSiA, with some that they calculated to be volatile.[17] The dominant ring-opening products ($C_6H_{20}O_8Si_5$ and $C_7H_{22}O_7Si_5$) in our study were identified as oxygenated volatile organic compounds (OVOCs) from a recent PAM-OFR study.[44] Additionally, as Avery et al.[44] performed their experiments at a much higher OH_{exp} (>1 × 10^{12} molecule cm^{-3} s), the largest signal in the SOA spectrum was identified to be $C_5H_{18}O_9Si_5$, which may generated from $C_6H_{20}O_8Si_5$ with the replacement of one CH_3 group with OH group. These ring-opening species are likely to be formed directly in the gas phase and partition into the particle phase. These gas/particle ring-opening phase products may also undergo further oxidation to form highly oxidized ring-opening products and thus contribute to the formation of SOSiA. Overall, our results indicate that the ring-opening compounds are mainly contributions to SOSiA formation from D_5. Recent studies have also suggested that ring-opening compounds are expected to be low in volatility, thus easily partitioning into the particle phase and appear to contribute significantly to SOA formation.[45] Wu and Johnston[17] also reported that most ring-opened D_5-SOSiA products are relatively nonvolatile.

It should be noted that the ring-opening products are more likely to deprotonate than protonate, and hence ESI-MS (−) allows better sensitivity for these compounds. However, the ESI-MS (+) mass spectra revealed more monomer products that were not detected with ESI-MS (−). The monomers were defined as the saturated products with exactly 5 Si atoms. Fig. S9† shows the possible structures of the identified monomers from the ESI-MS (+) mass spectra. The dominant monomers identified were $C_9H_{29}O_6Si_5$ and $C_{10}H_{31}O_6Si_5$ corresponding to one OH or CH_2OH substitution for a CH_3 group. The assigned formulae of monomers from our results indicate various functional group substitutions, where at least two CH_3 groups were replaced by OH and/or CH_2OH. The difference of observed products between our study and previous studies may related to the operation conditions of PAM (e.g., OH_{exp} conditions, initial precursor concentrations, residence time, humidity and aerosol seed). Wu and Johnston[17] performed their experiments at the OH_{exp} of 9 × 10^{10} molecule cm^{-3} s in their photo-oxidation chamber at a residence time of 15 minutes. Under low OH_{exp}, chemical composition of SOSiA may governed primarily by gas-phase OH oxidation of the precursors instead of heterogeneous oxidation of the condensed particles. In our study, we performed the experiments under a wider range of OH_{exp} (6.57 × 10^{10}–9.12 × 10^{11} molecule cm^{-3} s), the early-generation products are generally favored and the subsequently multi-generation products are also present. As discussed earlier, both the ring-opening products and the monomers are expected to be generated from successive oxidation processes.[11,21] Our results from the chemical composition characterization of SOSiA provide evidence that additional successive oxidation is important to make aerosols.

3.2.2. Effects of OH_{exp} on the chemical composition. Charan et al.[21] highlighted that the SOSiA yield strongly depends on OH_{exp}, which could range from 0–110%. To help interpret the large differences in SOSiA formation, we compared the representative ESI-MS mass spectra at the lowest, medium and highest OH_{exp}. As shown in Fig. 2, despite the product ion intensity differences, the same products were observed. The main differences in the mass spectra are the higher fractions of compounds with relatively small molecular masses in the m/z range of 200–300 under the lowest OH_{exp}, corresponding to small silanols, siloxandiols and their further oxidized products. The distribution of higher molecular weight D_5-SOA compounds remained largely constant under various OH_{exp} regimes, suggesting the ring-opening oxidation is an important SOSiA formation pathway in all cases. The oxidation mechanism should be considered in future work, as this knowledge is needed to confirm the structures of these products.

As shown in Fig. 2 and S10,† the most prominent mass spectra peak ($C_7H_{22}O_7Si_5$, defined as D_3T-OH–SiO_2) shifts to higher masses with a higher O : C ratio with the increase in OH_{exp} ($C_6H_{20}O_8Si_5$, defined as D_2T_2-(OH)$_2$–SiO_2), suggesting that additional oxidation contributes an important portion of the SOA. Wu and Johnston[25] found that additional oxidation leads mainly to the substitution of a CH_3 group by OH or CH_2OH for D_5 monomers and dimers. The dimers were defined as the saturated products with exactly 10 Si atoms. Although we did not observe the dimers, the same types of substitutions are observed for ring opening products (D_3T-OH–SiO_2, D_2T_2-(OH)$_2$–SiO_2 and D_2T_2-OH–CH_2OH–SiO_2 in Fig. S8†), meaning that the ring-opening products and their further oxidation products might undergo similar oxidation processes.

© 2023 The Author(s). Published by the Royal Society of Chemistry

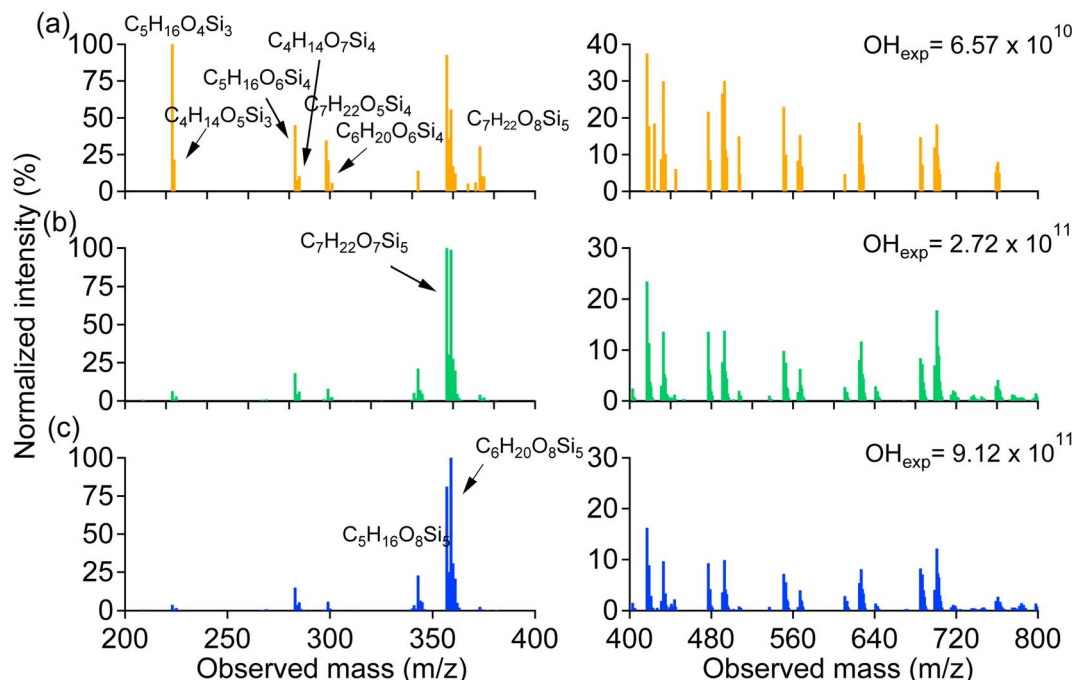*Environ. Sci.: Atmos.*, 2023, **3**, 662–671 | **667**

Fig. 2 Representative ESI-MS (−) mass spectrum of D_5-SOSiA at the lowest, medium and highest OH_{exp}. The molecular formulae are labeled in the m/z range of 200−400.

3.3. SOSiA formation mechanism

The SOSiA formation mechanism is outlined in Fig. 3 based on previous studies of siloxane oxidation chemistry and the main products identified in our work, which are discussed below. Oxidation is initiated through hydrogen abstraction by an OH radical from a methyl group, forming an alkyl radical (R_3SiCH_2), which quickly reacts with ambient oxygen to form a peroxy radical (RO_2).[9,41] Many different subsequent reactions of RO_2 are possible. For instance, the reactions of RO_2 can undergo a unique rearrangement leading to the formation of R_3SiOCH_2O radicals[8] or siloxy radicals (R_3SiO).[13] Fu et al.[13] suggested that
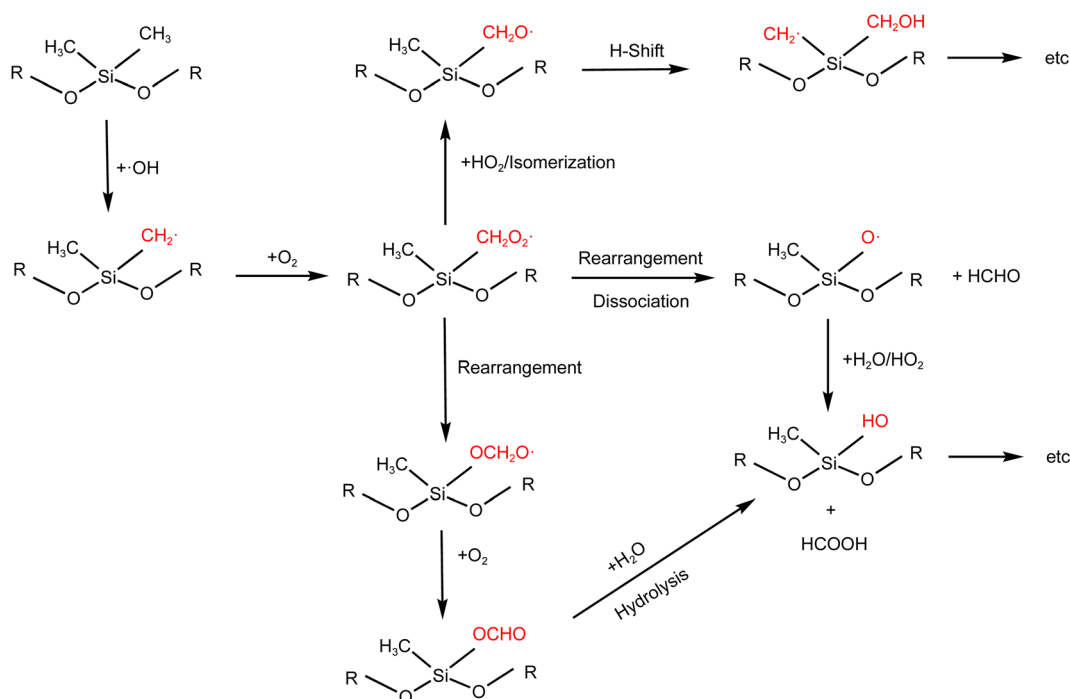

Fig. 3 Example reaction pathways of the OH-initiated oxidation of D_5-siloxane (R represents the either side of the central silicon atom).

formaldehyde (HCHO) is expected to be formed through the reactions. The R_3SiOCH_2O radical will react with O_2 to form the formate ester. The formate ester may undergo hydrolysis, leading to the formation of single substituted silanol (e.g., D_3T-OH) and formic acid (HCOOH).[24] Silanols could continue to hydrolyze to produce smaller silanols (e.g., DT-OH and D_2T-OH)[42] or undergo further reactions to produce siloxandiols (e.g., DT_2-$(OH)_2$ and D_2T_2-$(OH)_2$). In addition, the R_3SiO radical can also react with H_2O or HO_2 to make the silanol product;[11] although we did not observe D_5-silanol, its further oxidation products were identified (D_3T_2-$(OH)_2$, D_2T_3-$(OH)_3$ and DT_4-$(OH)_4$). Our results suggest that both reaction processes likely occurred. RO_2 can also react with HO_2 or undergo isomerization to form the alkoxy radical ($SiCH_2O$), which may also undergo H-shifts to generate silyl methanol products.[8,25] Although the silyl methanol product was not observed in this work, products with both silyl methanol groups and OH groups were identified (e.g., D_2T_3-$(OH)_2$–CH_2OH, DT_4-$(OH)_3$–CH_2OH and DT_4-OH–$(CH_2OH)_3$). In addition, we expect that ring-opening products (e.g., D_3T-OH–SiO_2, D_2T_2-$(OH)_2$–SiO_2 and D_2T_2-OH–CH_2OH–SiO_2) would partially follow a similar oxidation process, and the ring-opening products may further undergo oxidation reactions to form high-molecular-weight compounds. The detailed mechanisms need to be investigated in the future.

4. Conclusions

In this study, we generated SOSiA from the oxidation of D_5-siloxane over a wide range of OH_{exp}. We observed a series of high-molecular-weight SOSiA ions in the AMS mass spectra, which confirmed the ability of AMS to identify SOSiA composition. The technique demonstrated here can be used to track SOSiA-related species in the ambient environment in real time. The newly retrieved AMS ions ($C_wH_xO_ySi_z^+$) can be used as unique tracers for SOSiA, the related results can be used to estimate the relative contributions of SOSiA to total OA in the atmosphere. Molecular composition analysis shows that ring-opening products are a large portion of the SOA. Possible formation pathways of SOSiA are also proposed to better constrain the atmospheric chemistry of cVMS compounds. Future work should focus on the evaluation of calibration methods to better quantify the SOSiA species with AMS. Investigating SOSiA formation under variable conditions (e.g., different NO_x regimes and oxidants) should also be performed in future studies to better understand the oxidation mechanism of cVMS. Chamber simulation studies are also needed for a more detailed study of the kinetics involved in SOSiA formation.

Data availability

The data that support the findings of this study are available upon reasonable request from the authors.

Author contributions

H. Kim designed the project and experiments. Y. Chen, H. G. Kang, J. Jung, and Y. Park carried out the experiments. Y. Park performed the OH_{exp} calibration experiments. J. Jung conducted experiments and filter extraction. H. G. Kang participated in experiments for gas phase measurement. Y. Chen conducted the data analysis and prepared the manuscript. H. Kim contributed to manuscript improvement and supervised the project. All authors participated in discussions about the results.

Conflicts of interest

The authors declare that they have no conflict of interest.

Acknowledgements

References

1 B. C. McDonald, J. A. de Gouw, J. B. Gilman, S. H. Jathar, A. Akherati, C. D. Cappa, J. L. Jimenez, J. Lee-Taylor, P. L. Hayes, S. A. McKeen, Y. Y. Cui, S. W. Kim, D. R. Gentner, G. Isaacman-VanWertz, A. H. Goldstein, R. A. Harley, G. J. Frost, J. M. Roberts, T. B. Ryerson and M. Trainer, Volatile chemical products emerging as largest petrochemical source of urban organic emissions, *Science*, 2018, **359**, 760–764.

2 M. M. Coggon, B. C. McDonald, A. Vlasenko, P. R. Veres, F. Bernard, A. R. Koss, B. Yuan, J. B. Gilman, J. Peischl, K. C. Aikin, J. DuRant, C. Warneke, S. M. Li and J. A. de Gouw, Diurnal Variability and Emission Pattern of Decamethylcyclopentasiloxane (D5) from the Application of Personal Care Products in Two North American Cities, *Environ. Sci. Technol.*, 2018, **52**, 5610–5618.

3 X. Tang, P. K. Misztal, W. W. Nazaroff and A. H. Goldstein, Siloxanes Are the Most Abundant Volatile Organic Compound Emitted from Engineering Students in a Classroom, *Environ. Sci. Technol. Lett.*, 2015, **2**, 303–307.

4 M. M. Coggon, G. I. Gkatzelis, B. C. McDonald, J. B. Gilman, R. H. Schwantes, N. Abuhassan, K. C. Aikin, M. F. Arend, T. A. Berkoff, S. S. Brown, T. L. Campos, R. R. Dickerson, G. Gronoff, J. F. Hurley, G. Isaacman-VanWertz, A. R. Koss, M. Li, S. A. McKeen, F. Moshary, J. Peischl, V. Pospisilova, X. Ren, A. Wilson, Y. Wu, M. Trainer and C. Warneke, Volatile chemical product emissions enhance ozone and modulate urban chemistry, *Proc. Natl. Acad. Sci. U.S.A.*, 2021, **118**, e2026653118.

5 G. I. Gkatzelis, M. M. Coggon, B. C. McDonald, J. Peischl, K. C. Aikin, J. B. Gilman, M. Trainer and C. Warneke,

© 2023 The Author(s). Published by the Royal Society of Chemistry

Environ. Sci.: Atmos., 2023, **3**, 662–671 | **669**

Identifying Volatile Chemical Product Tracer Compounds in U.S. Cities, *Environ. Sci. Technol.*, 2021, **55**, 188–199.

6 S. Genualdi, T. Harner, Y. Cheng, M. MacLeod, K. M. Hansen, R. van Egmond, M. Shoeib and S. C. Lee, Global Distribution of Linear and Cyclic Volatile Methyl Siloxanes in Air, *Environ. Sci. Technol.*, 2011, **45**, 3349–3354.

7 X. Xiang, N. Liu, L. Xu and Y. Cai, Review of recent findings on occurrence and fates of siloxanes in environmental compartments, *Ecotoxicol. Environ. Saf.*, 2021, **224**, 112631.

8 R. Atkinson, E. C. Tuazon, E. S. C. Kwok, J. Arey, S. M. Aschmann and I. Bridier, Kinetics and products of the gas-phase reactions of (CH3)4Si, (CH3)3SiCH2OH, (CH3)3SiOSi(CH3)3 and (CD3)3SiOSi(CD3)3 with Cl atoms and OH radicals, *J. Chem. Soc. Faraday Trans.*, 1995, **91**, 3033–3039.

9 C. Rucker and K. Kummerer, Environmental chemistry of organosiloxanes, *Chem. Rev.*, 2015, **115**, 466–524.

10 R. Atkinson, Kinetics of the gas-phase reactions of a series of organosilicon compounds with hydroxyl and nitrate(NO3) radicals and ozone at 297 +- 2 K, *Environ. Sci. Technol.*, 1991, **25**, 863–866.

11 M. W. Alton and E. C. Browne, Atmospheric Degradation of Cyclic Volatile Methyl Siloxanes: Radical Chemistry and Oxidation Products, *ACS Environ. Au*, 2022, **2**, 263–274.

12 M. Qin, B. N. Murphy, K. K. Isaacs, B. C. McDonald, Q. Lu, S. A. McKeen, L. Koval, A. L. Robinson, C. Efstathiou, C. Allen and H. O. T. Pye, Criteria pollutant impacts of volatile chemical products informed by near-field modelling, *Nat. Sustain.*, 2021, **4**, 129–137.

13 Z. Fu, H. B. Xie, J. Elm, X. Guo, Z. Fu and J. Chen, Formation of Low-Volatile Products and Unexpected High Formaldehyde Yield from the Atmospheric Oxidation of Methylsiloxanes, *Environ. Sci. Technol.*, 2020, **54**, 7136–7145.

14 M. J. Whelan and J. Kim, Application of multimedia models for understanding the environmental behavior of volatile methylsiloxanes: Fate, transport, and bioaccumulation, *Integr. Environ. Assess. Manag.*, 2022, **18**, 599–621.

15 E. F. Katz, D. M. Lunderberg, W. L. Brown, D. A. Day, J. L. Jimenez, W. W. Nazaroff, A. H. Goldstein and P. F. DeCarlo, Large Emissions of Low-Volatility Siloxanes during Residential Oven Use, *Environ. Sci. Technol. Lett.*, 2021, **8**, 519–524.

16 P. Yao, E. Chianese, N. Kairys, R. Holzinger, D. Materić, C. Sirignano, A. Riccio, H. Ni, R.-J. Huang and U. Dusek, A large contribution of methylsiloxanes to particulate matter from ship emissions, *Environ. Int.*, 2022, **165**, 107324.

17 Y. Wu and M. V. Johnston, Aerosol Formation from OH Oxidation of the Volatile Cyclic Methyl Siloxane (cVMS) Decamethylcyclopentasiloxane, *Environ. Sci. Technol.*, 2017, **51**, 4445–4451.

18 R. Sommerlade, H. Parlar, D. Wrobel and P. Kochs, Product analysis and kinetics of the gas-phase reactions of selected organosilicon compounds with OH radicals using a smog chamber-mass spectrometer system, *Environ. Sci. Technol.*, 1993, **27**, 2435–2440.

19 E. Gallego, J. F. Perales, F. J. Roca, X. Guardino and E. Gadea, Volatile methyl siloxanes (VMS) concentrations in outdoor air of several Catalan urban areas, *Atmos. Environ.*, 2017, **155**, 108–118.

20 C. Han, H. Yang, K. Li, P. Lee, J. Liggio, A. Leithead and S. M. Li, Secondary organic aerosols from OH oxidation of cyclic volatile methyl siloxanes as an important Si source in the atmosphere, *Atmos. Chem. Phys.*, 2022, **22**, 10827–10839.

21 S. M. Charan, Y. Huang, R. S. Buenconsejo, Q. Li, D. R. Cocker III and J. H. Seinfeld, Secondary organic aerosol formation from the oxidation of decamethylcyclopentasiloxane at atmospherically relevant OH concentrations, *Atmos. Chem. Phys.*, 2022, **22**, 917–928.

22 L. H. Renbaum and G. D. Smith, Artifacts in measuring aerosol uptake kinetics: the roles of time, concentration and adsorption, *Atmos. Chem. Phys.*, 2011, **11**, 6881–6893.

23 N. J. Janechek, R. F. Marek, N. Bryngelson, A. Singh, R. L. Bullard, W. H. Brune and C. O. Stanier, Physical properties of secondary photochemical aerosol from OH oxidation of a cyclic siloxane, *Atmos. Chem. Phys.*, 2019, **19**, 1649–1664.

24 B. Chandramouli and R. M. Kamens, The photochemical formation and gas–particle partitioning of oxidation products of decamethyl cyclopentasiloxane and decamethyl tetrasiloxane in the atmosphere, *Atmos. Environ.*, 2001, **35**, 87–95.

25 Y. Wu and M. V. Johnston, Molecular Characterization of Secondary Aerosol from Oxidation of Cyclic Methylsiloxanes, *J. Am. Soc. Mass Spectrom.*, 2016, **27**, 402–409.

26 A. Milani, I. M. Al-Naiema and E. A. Stone, Detection of a secondary organic aerosol tracer derived from personal care products, *Atmos. Environ.*, 2021, **246**, 118078.

27 J. Xu, R. M. Harrison, C. Song, S. Hou, L. Wei, P. Fu, H. Li, W. Li and Z. Shi, PM2.5-bound silicon-containing secondary organic aerosols (Si-SOA) in Beijing ambient air, *Chemosphere*, 2022, **288**, 132377.

28 M. R. Canagaratna, J. T. Jayne, J. L. Jimenez, J. D. Allan, M. R. Alfarra, Q. Zhang, T. B. Onasch, F. Drewnick, H. Coe, A. Middlebrook, A. Delia, L. R. Williams, A. M. Trimborn, M. J. Northway, P. F. DeCarlo, C. E. Kolb, P. Davidovits and D. R. Worsnop, Chemical and microphysical characterization of ambient aerosols with the aerodyne aerosol mass spectrometer, *Mass Spectrom. Rev.*, 2007, **26**, 185–222.

29 A. T. Lambe, A. T. Ahern, L. R. Williams, J. G. Slowik, J. P. S. Wong, J. P. D. Abbatt, W. H. Brune, N. L. Ng, J. P. Wright, D. R. Croasdale, D. R. Worsnop, P. Davidovits and T. B. Onasch, Characterization of aerosol photooxidation flow reactors: heterogeneous oxidation, secondary organic aerosol formation and cloud condensation nuclei activity measurements, *Atmos. Meas. Tech.*, 2011, **4**, 445–461.

30 E. Kang, M. J. Root, D. W. Toohey and W. H. Brune, Introducing the concept of Potential Aerosol Mass (PAM), *Atmos. Chem. Phys.*, 2007, **7**, 5727–5744.

31 Z. Peng, D. A. Day, H. Stark, R. Li, J. Lee-Taylor, B. B. Palm, W. H. Brune and J. L. Jimenez, HOx radical chemistry in

670 | *Environ. Sci.: Atmos.*, 2023, **3**, 662–671

© 2023 The Author(s). Published by the Royal Society of Chemistry

oxidation flow reactors with low-pressure mercury lamps systematically examined by modeling, *Atmos. Meas. Tech.*, 2015, **8**, 4863–4890.

32 R. Li, B. B. Palm, A. M. Ortega, J. Hlywiak, W. Hu, Z. Peng, D. A. Day, C. Knote, W. H. Brune, J. A. de Gouw and J. L. Jimenez, Modeling the Radical Chemistry in an Oxidation Flow Reactor: Radical Formation and Recycling, Sensitivities, and the OH Exposure Estimation Equation, *J. Phys. Chem. A*, 2015, **119**, 4418–4432.

33 Z. Peng, D. A. Day, A. M. Ortega, B. B. Palm, W. Hu, H. Stark, R. Li, K. Tsigaridis, W. H. Brune and J. L. Jimenez, Non-OH chemistry in oxidation flow reactors for the study of atmospheric chemistry systematically examined by modeling, *Atmos. Chem. Phys.*, 2016, **16**, 4283–4305.

34 J. P. Rowe, A. T. Lambe and W. H. Brune, Technical Note: Effect of varying the $\lambda = 185$ and 254 nm photon flux ratio on radical generation in oxidation flow reactors, *Atmos. Chem. Phys.*, 2020, **20**, 13417–13424.

35 F. Bernard, D. K. Papanastasiou, V. C. Papadimitriou and J. B. Burkholder, Temperature Dependent Rate Coefficients for the Gas-Phase Reaction of the OH Radical with Linear (L2, L3) and Cyclic (D3, D4) Permethylsiloxanes, *J. Phys. Chem. A*, 2018, **122**, 4252–4264.

36 M. T. Timko, Z. Yu, J. Kroll, J. T. Jayne, D. R. Worsnop, R. C. Miake-Lye, T. B. Onasch, D. Liscinsky, T. W. Kirchstetter, H. Destaillats, A. L. Holder, J. D. Smith and K. R. Wilson, Sampling Artifacts from Conductive Silicone Tubing, *Aerosol Sci. Technol.*, 2009, **43**, 855–865.

37 A. Ballistreri, D. Garozzo and G. Montaudo, Mass spectral characterization and thermal decomposition mechanism of poly(dimethylsiloxane), *Macromolecules*, 1984, **17**, 1312–1315.

38 Z. Bibi, H. Coe, J. Brooks, P. I. Williams, E. Reyes-Villegas, M. Priestley, C. J. Percival and J. D. Allan, Technical note: A new approach to discriminate different black carbon sources by utilising fullerene and metals in positive matrix factorisation analysis of high-resolution soot particle

39 T. B. Onasch, E. C. Fortner, A. M. Trimborn, A. T. Lambe, A. J. Tiwari, L. C. Marr, J. C. Corbin, A. A. Mensah, L. R. Williams, P. Davidovits and D. R. Worsnop, Investigations of SP-AMS Carbon Ion Distributions as a Function of Refractory Black Carbon Particle Type, *Aerosol Sci. Technol.*, 2015, **49**, 409–422.

40 P. Liigand, K. Kaupmees, K. Haav, J. Liigand, I. Leito, M. Girod, R. Antoine and A. Kruve, Think Negative: Finding the Best Electrospray Ionization/MS Mode for Your Analyte, *Anal. Chem.*, 2017, **89**, 5665–5668.

41 S. J. Markgraf and J. R. Wells, The hydroxyl radical reaction rate constants and atmospheric reaction products of three siloxanes, *Int. J. Chem. Kinet.*, 1997, **29**, 445–451.

42 M. J. Whelan, E. Estrada and R. van Egmond, A modelling assessment of the atmospheric fate of volatile methyl siloxanes and their reaction products, *Chemosphere*, 2004, **57**, 1427–1437.

43 M. W. Alton and E. C. Browne, Atmospheric Chemistry of Volatile Methyl Siloxanes: Kinetics and Products of Oxidation by OH Radicals and Cl Atoms, *Environ. Sci. Technol.*, 2020, **54**, 5992–5999.

44 A. M. Avery, M. W. Alton, M. R. Canagaratna, J. E. Krechmer, D. T. Sueper, N. Bhattacharyya, L. Hildebrandt Ruiz, W. H. Brune and A. T. Lambe, Comparison of the Yield and Chemical Composition of Secondary Organic Aerosol Generated from the OH and Cl Oxidation of Decamethylcyclopentasiloxane, *ACS Earth Space Chem.*, 2023, **7**, 218–229.

45 A. Zaytsev, A. R. Koss, M. Breitenlechner, J. E. Krechmer, K. J. Nihill, C. Y. Lim, J. C. Rowe, J. L. Cox, J. Moss, J. R. Roscioli, M. R. Canagaratna, D. R. Worsnop, J. H. Kroll and F. N. Keutsch, Mechanistic study of the formation of ring-retaining and ring-opening products from the oxidation of aromatic compounds under urban atmospheric conditions, *Atmos. Chem. Phys.*, 2019, **19**, 15117–15129.